Rare-earth (Dy)-doped $(GeS_2)_{80}(In_2S_3)_{20}$ thin film: influence of annealing temperature in argon environment on the linear and nonlinear optical parameters

Pankaj Sharma[1] · Vineet Sharma[2] · Ekta Sharma[2] · A. Dahshan[3,4] · K. A. Aly[5,6] · Pawan Kumar[7] · Aslam Khan[8] · Ashok Kumar[1]

Abstract

We report the optical properties of thermally evaporated rare-earth (Dy) doped $(GeS_2)_{80}(In_2S_3)_{20}$ thin film. Film of thickness 1100 nm has been deposited on a microscopic glass slide, and the as-prepared thin film has been characterized using X-ray diffraction, energy dispersive spectroscopy and UV–visible–near infrared spectroscopy. With annealing temperature, the refractive index is noticed to decrease from 2.51 to 2.27, while the optical bandgap is observed to increase from 2.03 to 2.29. The dispersion of the refractive index n for as prepared and annealed thin films have discussed using the single oscillator model proposed by the Wemple–Di Domenico relationship. The observed value of E_o (5.31–4.40 eV) and dispersion energy E_d (28.22–18.18 eV) are decreasing for as prepared and annealed thin films. The increase of bandgap has been explained in terms of the disorder in the system.

Keywords Annealing · XRD · UV–visible–NIR spectroscopy · Thin film · Optical parameters

1 Introduction

The mid-infrared (MIR) comprises 3–25 μm spectral region and contains the significant atmospheric windows, i.e., 3–5 μm and 8–12 μm, and the molecular impressions of innumerable materials. To take advantage of the MIR region efficiently, the development of a large number of novel active and passive MIR fibres, sensors and components, narrow and broadband sources, comprising MIR lasers is required. The use of MIR lasers for a range of applications, including molecular spectroscopy, medical procedures, material processing and direct mid-infrared imaging is very significant. Rare-earth (RE) doped low phonon energy materials have revealed themselves to be competitive candidates for infrared lasers, amplifiers, and sources. Low phonon energy, in the range 50–650 cm^{-1}, is the characteristic of halide glasses and chalcogenide glasses, which is based on the composition. Unfortunately, the halide glasses are highly moisture absorptive and that makes them difficult to handle. On the other hand, are an attractive alternate as host material for these applications. Chalcogenide glasses which are low phonon glasses extend the superiority in terms of non-absorptive to moisture besides chemically and mechanically stable. Chalcogenide glasses have shown their remarkable electrical, optical and thermoelectric properties

✉ Pankaj Sharma
pks_phy@yahoo.co.in

1   Applied Science Department, National Institute of Technical Teachers Training and Research, Sector 26, Chandigarh 160019, India

2   Department of Physics and Materials Science, Jaypee University of Information Technology, Waknaghat, Solan, HP 173234, India

3   Department of Physics, Faculty of Science, King Khalid University, P.O. Box 9004, Abha, Saudi Arabia

4   Department of Physics, Faculty of Science, Port Said University, Port Said, Egypt

5   Department of Physics, Faculty of Science and Arts, Jeddah University, Jeddah, Saudi Arabia

6   Department of Physics, Faculty of Science, Al-Azhar University, Assiut Branch, Asyût, Egypt

7   School of Physics and Materials Science, Shoolini University, Solan, India

8   King Abdullah Institute for Nanotechnology, King Saud University, Riyadh 11451, Saudi Arabia

[1–8]. The small phonon energy of chalcogenide imprimatur a low possibility of multiphonon relaxation amongst the RE^{3+} energy levels, necessary for efficient RE^{3+} doped devices. Furthermore, these glasses can also be drawn to fibres.

Here, we report the dependence of the linear and nonlinear optical properties of thin films on the annealing temperature after the deposition for rare-earth-doped chalcogenide glass. To elucidate the annealing induced changes in optical properties transmission spectroscopy have been employed to witness the variations in bandgap and refractive index. Information derived in this paper can be fruitful for physical characterization of the films and understanding annealing temperature–properties correlations.

2 Experimental technique

The quaternary bulk samples of rare-earth (Dy) doped $(GeS_2)_{80}(In_2S_3)_{20}$ had been prepared by the conventional melt quenching approach from mixing of Ge, S, In and Dy elements with purity 99.999%. The elements Ge, S, In were weighed according to their atomic weight percentage and Dy by weight percentage with electrical balance and put inside the quartz ampoules. After that these ampoules sealed under the vacuum of 10^{-4} Pa, the ampoules were heated in step heating to a temperature 1100 °C. The melt was kept for 12 h at 1100 °C temperature for the homogeneity. After that the quenching of the ampoule was performed in ice-cooled water and afterwards ruptured to accumulate the prepared bulk samples. Thin films of the system under-investigated were prepared by utilizing thermal evaporation in vacuum coating unit, 12A4D in a high vacuum 10^{-5} mbar at room temperature. The pre cleaned glass substrate was used to deposit thin film in the molybdenum boat. The thickness of evaporated (Dy) doped $(GeS_2)_{80}(In_2S_3)_{20}$ thin films had been controlled by the thickness monitor DTM-101 using a quartz crystal. To study the optical changes, the as deposit thin film was annealed at 373, 423, 473 and 523 K argon environment for 2 h. The X-ray diffraction study shows amorphous nature of virgin and annealed thin films (Fig. 1). The transmission spectra of prepared thin film in the range 0–2.5 μm had been analyzed with the help of UV–Vis–NIR spectrophotometer. The thickness 1100 nm of the as deposit and annealed thin film has been estimated by the envelope method [9]. The composition of the samples has been verified by EDS ad found to have a variation of ± 5%.

3 Results and discussion

XRD patterns of annealed thin films have shown the origination of two peaks at $2\theta = 28°$ and 32.56°. It is observed that the reflection intensity increases with the rise of annealing temperature. The position of reflection peak at 28° is in good
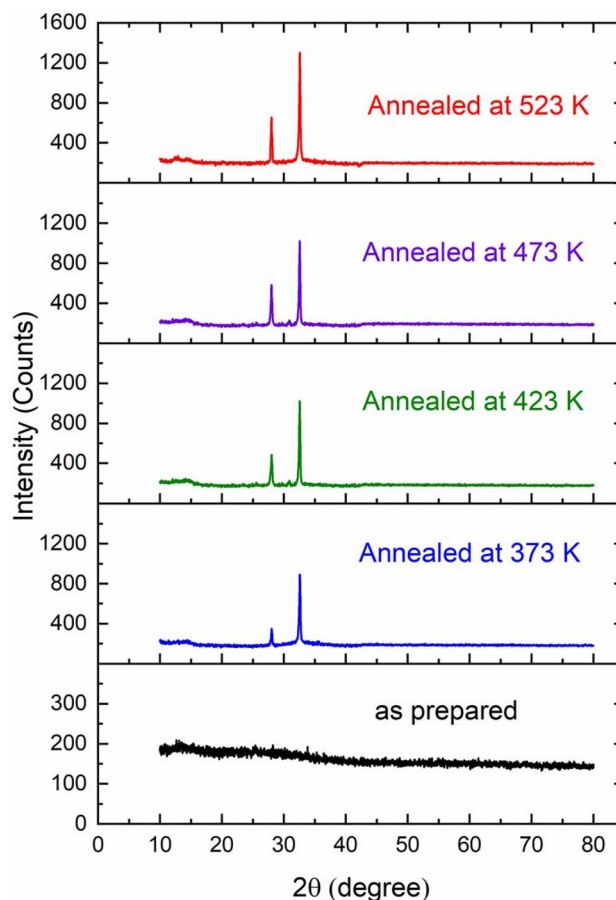
Fig. 1 XRD of as prepared and annealed (Dy) doped $(GeS_2)_{80}(In_2S_3)_{20}$ thin film

agreement with In_2S_3 [9]. The formation of reflection peak at 32.56° after annealing demonstrates the crystalline GeS_2 phase [10].

3.1 Linear optical parameters

3.1.1 Estimation of the refractive index and film thickness

The optical properties of thermally evaporated and annealed thin film at different heating rates have been utilized to estimate optical constants. The transmittance percentage of the as-prepared films shows significant increases after annealing at 373–523 K, whereas the film reflectance shows decreasing behaviour with the increase of annealing temperature, as shown in Fig. 2a. The interference fringes appear in the transmission and reflection spectra due to difference between the refractive index of thin film and the glass substrate. The refractive index and bandgap play very important role in the optoelectronics applications. The first approximate value of refractive index n_1 has been calculated by the Swanepoel method

[11] in the weak and medium absorption region ($\alpha \neq 0$ and $x < 1$, where α is the absorption coefficient and x is the absorbance) using the following expression: $n_1 = [M + (M^2 - s^2)^{0.5}]^{0.5}$, here $M = 2s\frac{T_M - T_m}{T_M T_m} + \frac{(s^2+1)}{2}$ and s is the refractive index of substrate whose value is calculated based on the measured substrate transmittance, T_s, using $s = (1/T_s) + [(1/T_s) - 1]^{0.5}$. The continuous envelope has formed on the transmission spectra, T_M and T_m refer to the maximum and minimum values of transmission at certain wavelength λ. These values of T_M and T_m can be taken from computer generated envelope. As and Example Fig. 2b shows the film transmittance for the as-prepared sample, the substrate transmittance, T_s, the generated transmission maxima T_M, transmission minima T_m, and the geometrical mean T_α.

The calculated value of the refractive index using the above equation is listed in Table 1. The basic interference equation is $2nd = m_o\lambda$ (m_o is the order number, integer for maxima and half-integer for minima). Let n_1, n_2 be the refractive indices at specific wavelengths at two adjacent maximum or minimum at λ_1 and λ_2 so that the thickness can be found as:

$$d = \frac{\lambda_1 \lambda_2}{2(\lambda_1 n_2 - \lambda_2 n_1)}. \tag{1}$$

The values of thickness d evaluated for as-deposited and annealed samples at different temperatures are listed as d_1 in Table 1. The average value of d_1 can be used along with calculated n_1 for the calculation of m_o using basic equation interference fringes. The accuracy of the thin film thickness can be noticeably enhanced by adopting an exact integer and half-integer value of m_o. By utilizing these m_o values, the new thickness or corrected thickness d_2 has been derived using the value of n_1. With the account of order number and d_2, the equation can be used to find n_2 at each λ. Thus the value of refractive n_2 obtained. The calculated values of n_2 can be fitted using a Cauchy dispersion relation: $n = a + \frac{b}{\lambda^2}$ which can be used for extrapolating the complete overall wavelengths. With the increase in annealing temperature, the refractive index n decreases, as shown in Fig. 3. This behaviour may be pointed out to the reduction of a number of unsaturated defects with annealing. Due to which the reduction in the localised density of states in the band structure consequently decreasing the indices of refraction. For successive maxima and minima starting from lesser energy or longer wavelength side the equation $2nd = m\lambda$ can be written as $\frac{I}{2} = 2d\left(\frac{n}{\lambda}\right) - m_1$, where $I = 0, 1, 2, 3\ldots$, where m_1 refers to the first tangent point. Figure 4 shows the plot of $(1/2)$ vs. (n/λ) a straight line with slope $2d$ and cut off a vertical axis at $-m_1$.

As represented in Fig. 2a, the absorption edge (strong absorption region, where the transmittance rapidly increases with increasing the wavelength) seems to shift towards short wavelengths, i.e., higher energy values with the increase annealing temperature. The absorption edge is located between 0 and 0.5 μm. This behaviour can be described in the wave vector, k-space of amorphous materials, through the direct and indirect electronic transition. These transitions occur from the interactions in the valence band (VB) between the light waves and electrons. Consequently, the electronics wave vector can alter the absorption edge and simultaneously encounters with lattice oscillations that are involved in indirect electronical transitions. Once sufficient energy is absorbed, the electron moves from valence band to conduction band. The increase in annealing temperature leads to a shift in the absorption edge towards lower wavelengths, i.e., blue shift. The later leads to an increase in the optical energy gap. Furthermore, with the rise of annealing temperature, the transmission of sample increases and reflectance decreases. The study of the refractive index is very much essential as the refractive index is an important optical parameter which is useful in linear and non-linear optical
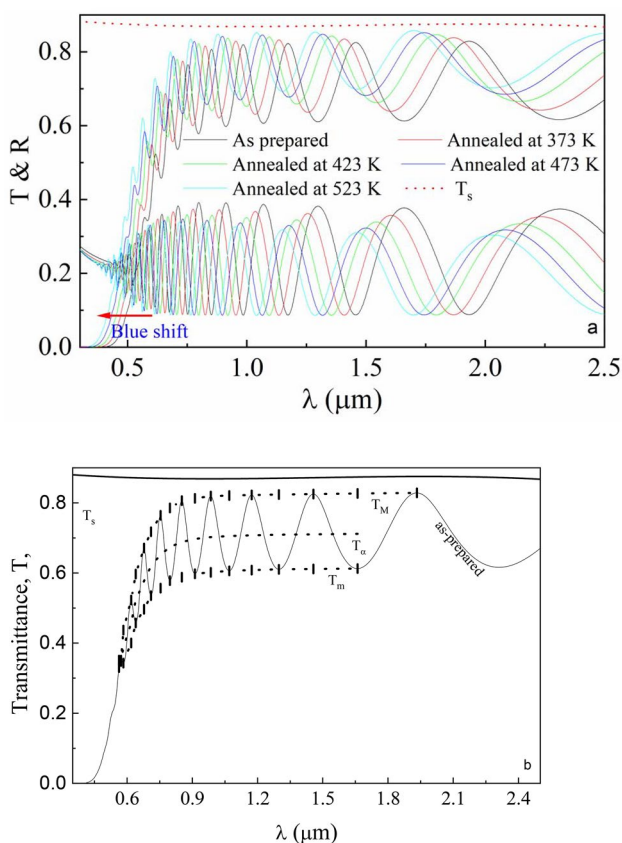

Fig. 2 a Transmission spectra of (Dy) doped $(GeS_2)_{80}(In_2S_3)_{20}$ thin film annealed at different temperature. **b** The film transmittance for the as-preapred film (as an example), the substrate transmittance, T_s, the generated transmission maxima T_M, transmission minima T_m, and the giometrical mean T_α

Table 1 Values of wavelength (λ), transmission maxima T_M, transmission minima T_m, refractive index of glass T_s, refractive index n_1, thickness d_1 (nm), order number m, corrected thickness d_2 (nm), refractive index n_2 from Cauchy relation for annealed (Dy) doped $(GeS_2)_{80}(In_2S_3)_{20}$ thin film

Sample	λ (nm)	T_M	T_m	T_s	n_1	d_1 (nm)	m_o	m	d_2 (nm)	n_2
Asprepared	1660	0.83	0.61	0.87	2.51	–	3.54	3.5	1156	2.53
	1457	0.83	0.61	0.87	2.52	1154	3.84	4	1156	2.54
	1298	0.82	0.61	0.87	2.53	1149	4.32	4.5	1155	2.55
	1173	0.82	0.61	0.87	2.54	1160	4.80	5	1156	2.56
	1070	0.82	0.61	0.87	2.54	1164	5.27	5.5	1156	2.57
	985	0.82	0.60	0.87	2.56	1139	5.76	6	1155	2.58
	912	0.81	0.60	0.87	2.56	1185	6.23	6.5	1157	2.59
	852	0.81	0.59	0.87	2.59	1102	6.73	7	1153	2.60
	797	0.79	0.58	0.87	2.58	1254	7.17	7.5	1159	2.61
	754	0.76	0.56	0.87	2.62	1038	7.71	8	1151	2.63
	710	0.72	0.54	0.87	2.60	1344	8.12	8.5	1161	2.63
	678	0.67	0.50	0.87	2.67	–	8.72	9	1144	2.66
	640	0.60	0.46	0.87	2.65	–	9.17	9.5	1149	2.65

$\bar{d}_1 = 1169, \delta_1 = 44\,\text{nm}(3.74\%), \bar{d}_2 = 1154, \delta_2 = 4.48\,\text{nm}(0.38\%)$

Sample	λ (nm)	T_M	T_m	T_s	n_1	d_1 (nm)	m_o	m	d_2 (nm)	n_2
Annealed at 373 K	1602	0.84	0.64	0.87	2.44	–	3.50	3.5	1147	2.45
	1407	0.84	0.64	0.87	2.45	1149	4.00	4	1147	2.46
	1254	0.84	0.64	0.87	2.46	1142	4.51	4.5	1147	2.47
	1133	0.84	0.63	0.87	2.47	1143	5.01	5	1146	2.48
	1034	0.83	0.63	0.87	2.48	1155	5.50	5.5	1147	2.49
	952	0.83	0.63	0.87	2.49	1124	6.01	6	1145	2.50
	882	0.83	0.62	0.87	2.50	1179	6.50	6.5	1148	2.51
	824	0.82	0.61	0.87	2.52	1086	7.03	7	1143	2.52
	771	0.80	0.60	0.87	2.52	1233	7.50	7.5	1149	2.53
	730	0.78	0.58	0.87	2.56	1042	8.05	8	1141	2.55
	687	0.73	0.56	0.87	2.54	1275	8.50	8.5	1148	2.55
	657	0.69	0.52	0.87	2.60	–	9.10	9	1135	2.59
	621	0.62	0.48	0.87	2.59	–	9.57	9.5	1139	2.58

$\bar{d}_1 = 1139, \delta_1 = 54.1\,\text{nm}(4.75\%), \bar{d}_2 = 1143, \delta_2 = 2.36\,\text{nm}(0.21\%)$

Sample	λ (nm)	T_M	T_m	T_s	n_1	d_1 (nm)	m_o	m	d_2 (nm)	n_2
Annealed at 423 K	1796	0.85	0.66	0.87	2.39	–	2.99	3	1129	2.40
	1543	0.84	0.66	0.87	2.40	1115	3.49	3.5	1127	2.40
	1356	0.84	0.66	0.87	2.41	1128	3.99	4	1127	2.41
	1209	0.84	0.66	0.87	2.42	1119	4.49	4.5	1126	2.42
	1094	0.84	0.66	0.87	2.43	1134	4.99	5	1127	2.44
	998	0.84	0.65	0.87	2.44	1128	5.49	5.5	1127	2.44
	921	0.84	0.65	0.87	2.45	1126	5.99	6	1127	2.46
	853	0.83	0.64	0.87	2.46	1152	6.48	6.5	1129	2.47
	799	0.82	0.63	0.87	2.48	1097	6.99	7	1127	2.49
	748	0.80	0.62	0.87	2.48	1213	7.45	7.5	1132	2.50
	708	0.78	0.59	0.87	2.52	1018	7.45	7.5	1132	2.50
	667	0.74	0.57	0.87	2.51	1264	8.01	8	1124	2.52

$\bar{d}_1 = 1125, \delta_1 = 62.39\,\text{nm}(3.55\%), \bar{d}_2 = 1127, \delta_2 = 1.99\,\text{nm}(0.16\%)$

Sample	λ (nm)	T_M	T_m	T_s	n_1	d_1 (nm)	m_o	m	d_2 (nm)	n_2
Annealed at 473 K	1499	0.86	0.68	0.87	2.34	–	3.54	3.5	1119	2.35
	1319	0.86	0.68	0.87	2.35	1130	4.04	4	1120	2.36
	1176	0.86	0.67	0.87	2.36	1109	4.56	4.5	1119	2.37
	1065	0.85	0.67	0.87	2.38	1128	5.06	5	1120	2.39
	973	0.85	0.67	0.87	2.39	1131	5.56	5.5	1121	2.40
	898	0.85	0.66	0.87	2.41	1109	6.07	6	1120	2.41
	833	0.84	0.65	0.87	2.41	1156	6.56	6.5	1123	2.43
	780	0.84	0.64	0.87	2.44	1073	7.09	7	1119	2.45
	731	0.82	0.63	0.87	2.44	–	7.56	7.5	1124	2.46
	692	0.80	0.61	0.87	2.48	–	8.12	8	1116	2.48

Table 1 (continued)

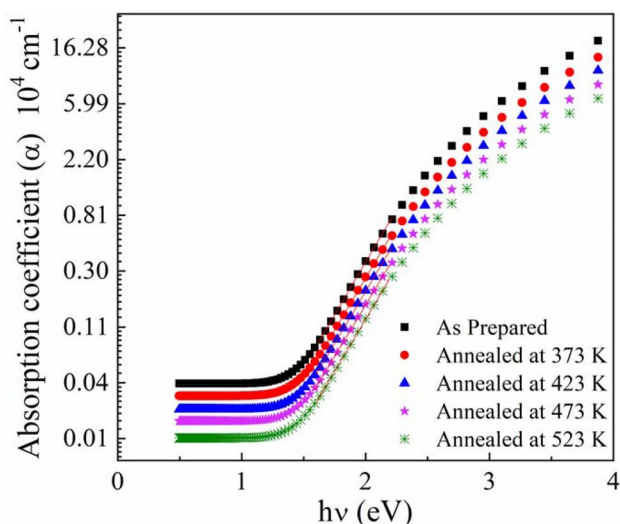| Sample	λ (nm)	T_M	T_m	T_s	n_1	d_1 (nm)	m_o	m	d_2 (nm)	n_2
$\bar{d}_1 = 1119, \delta_1 = 36\,\text{nm}(3.24\%), \bar{d}_2 = 1116, \delta_2 = 10\,\text{nm}(0.91\%)$										
Annealed at 523 K	1701	0.86	0.70	0.87	2.29	–	3.00	3	1115	2.29
	1463	0.86	0.70	0.87	2.30	1102	3.51	3.5	1113	2.30
	1287	0.85	0.70	0.87	2.31	1114	4.01	4	1113	2.31
	1149	0.85	0.69	0.87	2.32	1108	4.51	4.5	1113	2.32
	1042	0.85	0.69	0.87	2.34	1130	5.01	5	1114	2.34
	952	0.85	0.68	0.87	2.35	1116	5.51	5.5	1115	2.35
	880	0.85	0.68	0.87	2.37	1117	6.01	6	1115	2.37
	816	0.84	0.67	0.87	2.38	1131	6.50	6.5	1116	2.38
	765	0.84	0.66	0.87	2.40	1085	7.01	7	1114	2.40
	718	0.82	0.65	0.87	2.41	1198	7.48	7.5	1119	2.42
	681	0.80	0.62	0.87	2.44	1052	8.01	8	1115	2.45
	643	0.76	0.60	0.87	2.44	1203	8.47	8.5	1119	2.45
	616	0.73	0.57	0.87	2.49	1024	9.02	9	1114	2.49
	584	0.67	0.53	0.87	2.49	–	9.51	9.5	1115	2.49
$\bar{d}_1 = 1115, \delta_1 = 51\,\text{nm}(4.56\%), \bar{d}_2 = 1114, \delta_2 = 1.97\,\text{nm}(0.98\%)$										
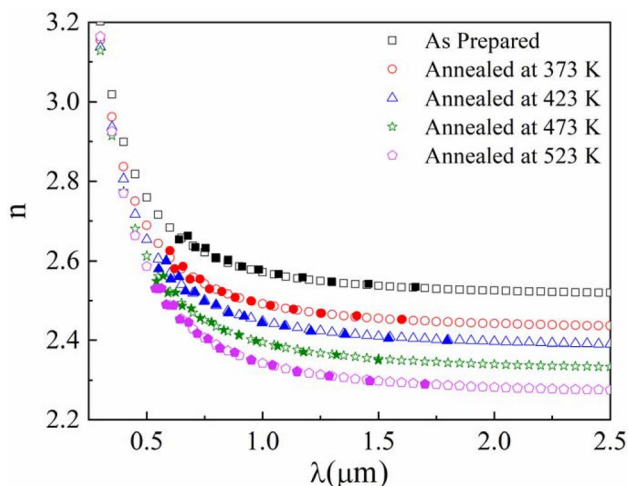
Fig. 3 Variation of refractive index (n) with the wavelength for annealed (Dy) doped $(GeS_2)_{80}(In_2S_3)_{20}$ thin film

Fig. 4 Plots of l/2 vs. n/λ to determine the film thickness and the first order number m_1 for as prepared and annealed for (Dy) doped $(GeS_2)_{80}(In_2S_3)_{20}$ thin film

phenomenon. The optical absorption spectra are essential for determining the absorption strength of films and evaluating the optical band structure of solid materials. The absorption coefficient α can be calculated as: $\alpha = \frac{1}{d}\ln\left(\frac{1}{x}\right)$, where x is the absorbance, d refers to thin-film thickness in cm. The variation of α with the photon energy is shown in Fig. 5. The as-prepared thin film shows strong absorption edge in the longer wavelength region, whereas the absorption coefficient for annealed film is decreased. This remarkable decrease in absorption coefficient is consistence with the enhancement of transmittance, and it can be attributed that there is a structural improvement by the increasing annealing temperature. With the increase in photon energy, the absorption

coefficient of all the films as prepared and annealed increases. But this rate of change is influenced by the parameter optical bandgap energy. If the photon energy is higher than bandgap energy, then there is an increase in the value of the absorption coefficient with the decrease in wavelength. However, if the photon energy is lower than the bandgap energy then α is small, then the material is transparent. Although the value of absorption index k is directly dependent on α and both parameters follow the same trend with wavelength. The complex refractive index: $\tilde{n} = n - ik$

Fig. 5 Dependence of absorption coefficient (α) with photon energy

Fig. 6 Variation of extinction coefficient (k) with wavelength for (Dy) doped $(GeS_2)_{80}(In_2S_3)_{20}$ thin film annealed at different temperature
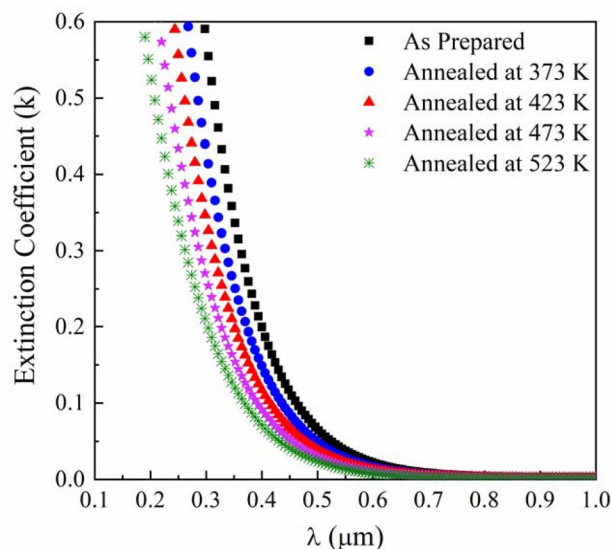
is used for the determination of the speed of an electromagnetic wave propagate within any material. The optical constant k is known as attenuation coefficient, extinction coefficient or absorption index describes the fall in the amplitude of the electromagnetic wave oscillation. Hence k has a crucial role in the describing the propagation of electromagnetic lightwave, and its value indicates the dissipation in light energy. The extinction coefficient is calculated by the relation:

$$k = \frac{\alpha \lambda}{4\pi}. \tag{2}$$

Both absorption coefficient and extinction coefficient show a decrease with the increase in annealing temperature, as shown in Figs. 5 and 6, respectively. The optical constant refractive index n and extinction coefficient k is affected by the annealing temperature.
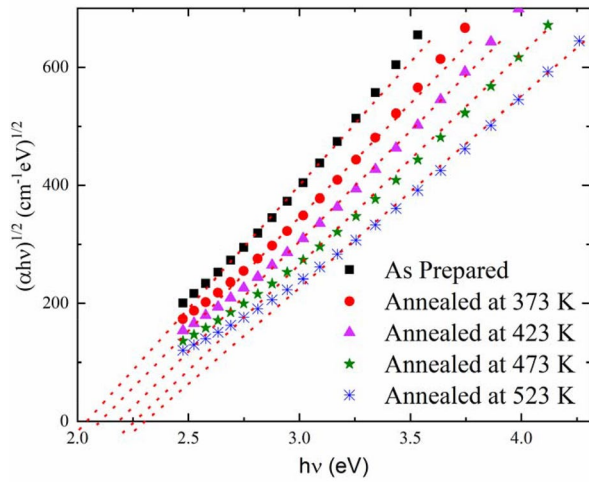
3.1.2 Calculation of optical bandgap

The absorption process which occurs between lowest energy of the conduction band (LECB) and high energy of valence band (HECB) with the photon assistance in amorphous semiconducting materials is described as an indirect allowed transition. Based on the α values the absorption spectrum has been divided into three regions: the first region for $\alpha < 0$ cm^{-1} (below bandgap absorption); the second region for $10 < \alpha < 10^4$ cm^{-1} (Urbach tails); and the third region for $\alpha > 10^4$ cm^{-1} (interband high absorption). The optical bandgap of as-prepared and annealed thin films have been evaluated by the Tauc relation [12]:

$$\alpha h\upsilon = B(h\upsilon - E_g)^y, \tag{3}$$

where α is the absorption coefficient, B refers to the slope of Tauc's edge also known as band tailing parameter and indicates the degree of structural randomness of amorphous semiconductors, E_g denotes the optical bandgap, and $h\upsilon$ refers to the photon energy. As discussed earlier, the transition type is indirect allowed transitions, so $y = 2$. The Tauc plot in Fig. 7 shows the variation of $(\alpha h\upsilon)^{0.5}$ and the photon energy $h\upsilon$(eV). This behaviour is in good agreement with a large published data [13–21]. The energy bandgap has been found by extrapolating the linear portion for these plots to intercept the photon energy. With the increase in annealing temperature, the absorption edge shifted towards lower wavelength, which leads to an increase in the optical bandgap. The response E_g can be understood through the Mott and Davis model [22]. This model suggested that the optical bandgap is indirectly proportional to the defects and width of the localized states. The increase of annealing temperature up to transition temperature T_g reduces the defects and disorder in the system which leads to reduction of width of localized states in the band structure, consequently it results in an increase in the bandgap. This has also been observed in XRD as the crystallinity improves with increase in annealing temperature (Fig. 1). In some amorphous chalcogenide, the reduced density of homopolar bonds has proposed to contribute to a blue shift of a gap. The increase in optical bandgap with rise in annealing temperature has also been observed in other chalcogenide glasses [23–25].

Fig. 7 Plot of $(\alpha h\upsilon)^{0.5}$ vs. photon energy for as prepared and annealed thin film

Fig. 8 Plot between $(n^2 - 1)^{-1}$ vs. $(h\upsilon)^2$ for (Dy) doped $(GeS_2)_{80}(In_2S_3)_{20}$ thin film annealed at different temperature

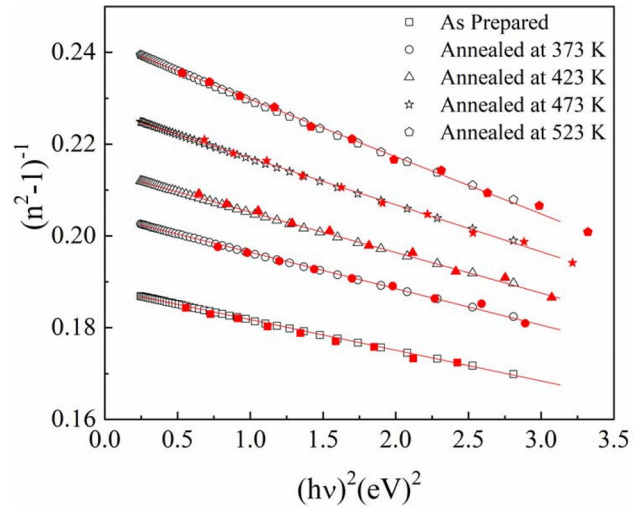### 3.1.3 Determination of single oscillator parameters by WDD model

The dispersion parameters play an essential role in the optical phenomenon. The dispersion refractive index of as-prepared and annealed film has been analyzed according to a single oscillator model suggested by Wemple–Di Domenico (WDD) by the formula [26, 27]:

$$n^2 - 1 = \frac{E_o E_d}{E_o^2 - (h\upsilon)^2}. \tag{4}$$

Reformulating the equation:

$$(n^2 - 1)^{-1} = \frac{[E_o^2 - (h\upsilon)^2]}{E_o E_d} = \frac{E_o}{E_d} - \frac{(h\upsilon)^2}{E_o E_d}, \tag{5}$$

where E_d is the dispersion energy, which measures the strength of interband photon transition and E_o refers to the single oscillator energy identified as average energy gap The approximation of WDD theory and a single oscillator model has been applied to realize the many optical data. The dispersion parameters (E_o and E_d) do not depend on each other. Several optical constants may be calculated from these values like the static refractive index n_o etc. From the linear fit of Fig. 8, the slope represents $(E_o E_d)^{-1}$ and the intercept of the vertical axis determines E_o/E_d. The values of E_o and E_d are listed in Table 2. It has been noted that with the increase in annealing temperature, there is a decrease in both E_o and E_d values. The known dispersion energy values (E_o and E_d) have been used to find the lattice dielectric constant, i.e., zero frequency dielectric constant ε_o and n_o via a relation:

$$\varepsilon_o = n_o^2 \text{ and } n_o = \left[1 + \frac{E_d}{E_o}\right]^{0.5}.$$

The calculated values of the above two parameters lattice dielectric constant ε_L and refractive index n_o are given in Table 2. The static refractive index values show decreases value from 2.51 to 2.27. In contrast, the zero frequency dielectric constant values decrease from 6.32 to 5.13 with the increase of annealing temperature from as-prepared thin films at 523 K. However, the ratio of single oscillator energy E_o and optical bandgap energy E_g has been computed and listed in Table 2. Tanaka [28] suggested that this ratio of E_o/E_g values is almost equal to 2. In the present study, this ratio varies from 2.61 (for as prepared sample) to 1.92 (for sample annealed at 523 K). It should be kept in mind that the above relationship given by Tanaka opt for the indirect transitions.

3.1.4 Computation of Sellmeier oscillator parameters

Sellmeier determined that in the Vis NIR spectral range the optical refractive depends substantially on the wavelength. The interband oscillator wavelength λ_o and oscillator strength S for composition thin films at different annealing temperature is calculated as [29, 30]:

$$\left(n^2 - 1\right)^{-1} = \frac{1}{(n_o^2 - 1)} - \frac{1}{(n_o^2 - 1)}\left(\frac{\lambda_o}{\lambda}\right)^2 \tag{6}$$

$$\left(\frac{n_o^2 - 1}{n^2 - 1}\right) = 1 - \left(\frac{\lambda_o}{\lambda}\right)^2,$$

whereas it is known that the speed of light is defined as the product of wavelength and frequency ($c = \upsilon\lambda$) and using Planck equation $E = h\upsilon$, $\lambda = hc/h\upsilon$.

Table 2 Values of single oscillator energy (E_o), dispersion energy (E_d), static refractive index (n_o), optical bandgap (E_g), Sellmeier parameters (λ_o and S), lattice dielectric constant (ε_L), plasma frequency (ω_p)

Sample	E_d eV	E_o	E_g	n_o	ε_L	E_o/E_g	λ_o nm	S 10^{13} m^2	ω_p 10^{13} Hz	N/m^* 10^{52} g^{-1} cm^{-3}
As prepared	28.22	5.31	2.03	2.51	6.32	2.61	234	9.69	4.35	5.19
Annealed at 373 K	24.85	5.07	2.09	2.43	5.90	2.42	245	8.15	4.37	5.25
Annealed at 423 K	23.02	4.93	2.18	2.38	5.67	2.26	252	7.34	4.43	5.38
Annealed at 473 K	20.75	4.71	2.26	2.32	5.41	2.08	264	6.33	4.50	5.57
Annealed at 523 K	18.18	4.40	2.29	2.27	5.13	1.92	283	5.18	4.71	6.10

Therefore, the above equation becomes

$$\left(n^2 - 1\right)^{-1} = \frac{1}{(n_o^2 - 1)} - \frac{h\upsilon^2}{(n_o^2 - 1)hc^2}\lambda_o^2.$$

By comparing the WDD equation and the above equation:

$$\frac{1}{(n_o^2 - 1)} = \frac{E_o}{E_d} \quad \text{and} \quad \frac{1}{(n_o^2 - 1)}\lambda_o^2\frac{(h\upsilon)^2}{(hc)^2} = \frac{(h\upsilon)^2}{E_d E_o}.$$

Therefore, $\frac{1}{(n_o^2-1)} = \frac{E_o}{E_d}$ and $\frac{1}{(n_o^2-1)}\frac{\lambda_o^2}{(hc)^2} = \frac{1}{E_d E_o}$.

By simplifying above equation becomes:

$$E_o = \frac{hc}{\lambda_o} \quad \text{and} \quad E_d = (n_o^2 - 1)\frac{hc}{\lambda_o}$$

$$\frac{E_d}{E_o} = (n_o^2 - 1)\frac{hc}{\lambda_o} \times \frac{\lambda_o}{hc} = (n_o^2 - 1) \quad \text{so } S = \frac{(n_o^2 - 1)}{\lambda_o^2} = \frac{E_d/E_o}{\lambda_o^2}. \tag{7}$$

Hence, on the basis of the formerly calculated single oscillator parameters (E_o and E_d) the strength and wavelength of an oscillator (S and λ_o) can be easily determined. The calculated values of λ_o and S are listed in Table 2. It is clear from the table that the value of λ_o increased from 234 nm to 283 nm, on contrary S values decreases from 9.69×10^{13} m^{-2} to 5.18×10^{13} m^{-2} as the increase of annealing temperature. The λ_o and S show the variation with changing the thermal annealing. These variations predict that the film is suitable for varying the refractive index and oscillator parameter by thermal annealing.

The lattice dielectric constant (ε_L) rises mainly due to two factors, i.e., partially due to the bound electrons and partly of the free electrons. The refractive index on lattice dielectric constant with wavelength has been represented as [22, 29]:

$$n^2 = \varepsilon_\infty = \varepsilon_L - \left[\frac{e^2}{4\pi c^2\varepsilon_0}\frac{N}{m^*}\right]\lambda^2, \tag{8}$$

where c is the velocity of light in the vacuum, e denotes the electronic charge, ε_o refers to the permittivity in free space and N and m^* corresponds to the number of carrier concentration and effective mass, respectively. Figure 9 shows the plots of n^2 vs. λ^2 for the different annealing temperatures.

The values of (N/m^*) and ε_L have been estimated through the intercept and slope of the curve by extrapolating $\lambda^2 \rightarrow 0$ in the graph. The calculated values of (N/m^*) and ε_L have been listed in Table 2.

3.1.5 Plasma frequency

From Drude's model of dielectric materials, the plasma frequency ω_p has been calculated by the parameter (N/m^*), the electric permittivity of air (ε_o), high-frequency dielectric constant (ε_∞) and the electronic charge (e) from the relation [29, 31]:

$$\omega_p^2 = \left(\frac{e^2}{\varepsilon_0\varepsilon_\infty}\right)\left(\frac{N}{m^*}\right). \tag{9}$$

The value of ε_∞ has been calculated in Eq. 8. The calculated values of ω_p have been listed in Table 2. It has been noticed that with the increase in annealing temperature, the plasma frequency ω_p increases from 4.35×10^{13} Hz to 4.71×10^{13} Hz. These exorbitant values of ω_p are ascribed to the more values of the free carrier concentrations.
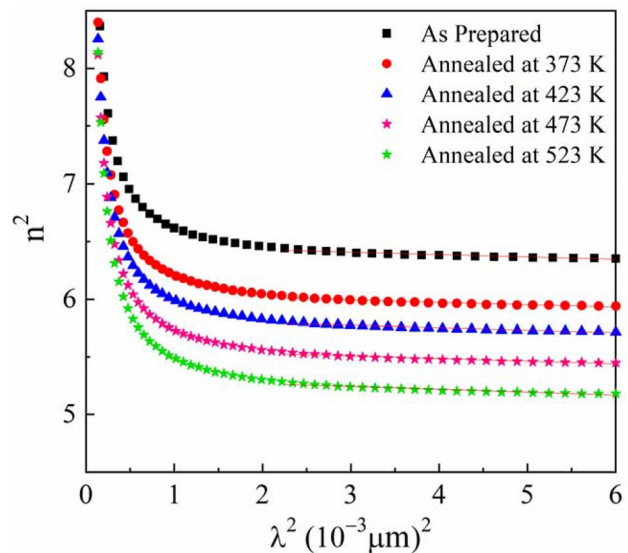
Fig. 9 Variation of ε_2 with λ^2 for as prepared and annealed thin film

3.2 Nonlinear optical parameters

In chalcogenide-based materials, the nonlinear behaviour occurs due to the interaction of nucleus with electronic polarizability, which further affects the bond length. Under very high electric field the material is no longer polarized linearly with electric field, but it gets proportional with the square of electric field. Due to high field interaction, the change in the index of refraction takes place according to the relation: $\Delta n = n_2 |E|^2$ here, n_2, Δn and E are nonlinear refractive index, change in index of refraction due to high electric field and electric field. The relationship between linear and third-order nonlinear susceptibility consisting of WDD parameters and average energy gap has been proposed by Wang [32]. The third-order nonlinearity ($\chi^{(3)}$) is treated as the lowest order nonlinearity leading in all glassy materials.

Ticha Tichy proposed a semi empirical relation for the determination of nonlinear refractive index n$_2$ with the combination of Miller's generalized relationship [32, 33] and WDD single oscillator model. According to these relations, the nonlinear susceptibility ($\chi^{(3)}$) is measured in esu using the relation [34]: $\chi^{(3)} = Z(\chi^1)^4$, where for chalcogenide glasses, $\chi^1 = (n^2 - 1)\big/4\pi$ at ($h\upsilon \to 0$ and n = n$_o$) for the prediction of values of refractive index as well as ($\chi^{(3)}$)

$$\chi^{(3)} = Z \left[\frac{E_d}{4\pi E_o} \right]^4. \tag{10}$$

Here, Z is constant having value 1.7×10^{-10} esu. The nonlinear refractive index can be estimated as

$$n_2 = \frac{12\pi \chi^{(3)}}{n_o}, \tag{11}$$

where n_o refers to the static refractive index as computed through WDD model in Table 3. It is clear from Table 3 that the nonlinear refractive index n_2 follow the same trend as that of linear refractive index n_2. The values of third-order nonlinear susceptibility ($\chi^{(3)}$) and the nonlinear refractive index n_2 decrease with the increasing annealing temperature.

The critical optical properties refractive index and bandgap play a vital role in the optoelectronic applications such as photodiodes, optical fibres and light-emitting diodes. In literature, the inverse relationship has been found between both the two parameters. The refractive index can be calculated theoretically on the basis of the bandgap using some relations. The most common used relations are Moss [35] and Ravindra et.al relation [34]. According to Moss model the energy levels of the electrons in solids are scaled down by a factor $^1/_{n^4}$. The Moss relation is as follow [35]: $n_{\text{Moss}}^4 E_g = p$ eV or $n_{\text{Moss}} = \left(p/E_g\right)^{0.25}$, where the value $p = 95$ eV and n, E_g is the refractive index and energy gap of as-deposited and annealed thin film calculated above by

Table 3 Third-order nonlinear susceptibility ($\chi^{(3)}$) and nonlinear refractive index (n_2)

Sample	($\chi^{(3)}$) 10^{-12} esu	n_2 10^{-11} esu	n_{exp}	n_{Moss}	n_{Ravindra}
As prepared	3.22	4.82	2.65	2.64	2.72
Annealed at 373 K	2.32	3.60	2.58	2.58	2.66
Annealed at 423 K	1.92	3.03	2.52	2.54	2.62
Annealed at 473 K	1.51	2.45	2.48	2.49	2.57
Annealed at 523 K	1.17	1.95	2.45	2.43	2.51

Theoretical values of refractive index (n_{Moss} and n_{Ravindra})

Swanepoel and Tauc method. The Moss relation is modified by Ravindra et al. by suggesting another value of $p = 108$ eV. The relation is as follows [36, 37]:

$$n_{\text{Ravindra}}^4 E_g = 108 \text{ eV}. \tag{12}$$

The obtained theoretical values of refractive index using the above models are listed in Table 3. These obtained values of the refractive index follow the same trend as the experiment value of the refractive index.

4 Conclusion

X-ray diffraction, energy dispersive spectroscopy and UV–visible–near infrared spectroscopy has been used to examine the structural and optical properties of the as-deposited and annealed (Dy) doped (GeS$_2$)$_{80}$(In$_2$S$_3$)$_{20}$ thin film. The transmission increased, whereas the refractive index and absorption coefficient decreased with thermal annealing. All the calculated parameters demonstrated a good response to the heat treatment. The dispersion parameters E_o, E_d, n_o, decreases with the increasing annealing temperature, whereas as the λ_0, bandgap increases with the annealing temperature. The nonlinear refractive index and nonlinear susceptibility also decreases of as-deposited and annealed thin films. As the refractive index have value $n > 2$ for as-deposited and annealed thin film so these may be used for NIR imaging.

References

1. D.C. Sati, A. Dahshan, P. Sharma, Appl. Mater. Today **17**, 142–158 (2019)

2. V. Sharma, S. Sharda, N. Sharma, S.C. Katyal, P. Sharma, Prog. Solid State Chem. **54**, 31–44 (2019)

3. K.A. Aly, Y. Saddeek, A. Dahshan, Appl. Phys. A Mater. Sci. Process. **122**(3), 1–6 (2016)

4. K.A. Aly, J. Non Cryst. Solids **355**(28–30), 1489–1495 (2009)

5. A. Dahshan, S.R. Alharbi, K.A. Aly, Y. Saddeek, J. Therm. Anal. Calorim. **140**(1), 125–131 (2020)

6. P. Sharma, A. Dahshan, V.K. Sehgal, K.A. Aly, IEEE Trans. Electron Devices **65**(8), 3408–3413 (2018)

7. P. Sharma, N. Sharma, S. Sharda, S.C. Katyal, V. Sharma, Prog. Solid State Chem. **44**(4), 131–141 (2016)

8. S. Chand, E. Sharma, P. Sharma, J. Alloy. Compd. **770**, 1173–1180 (2019)

9. Z. Li, C. Lin, Q. Nie, S. Dai, J. Am. Ceram. Soc. **96**(1), 125–129 (2013)

10. M.J. MacLachlan, S. Petrov, R.L. Bedard, I. Manners, G.A. Ozin, Angew. Chem. Int. Ed. **37**(15), 2075–2079 (1998)

11. R. Swanepoel, J. Phys. E Sci. Instrum. **16**(12), 1214–1222 (1983)

12. J. Tauc, Mater. Res. Bull. **3**(1), 37–46 (1968)

13. K.A. Aly, Y.B. Saddeek, A. Dahshan, Opt. Mater. **109**, 110341 (2020)

14. H.H. Hegazy, A. Dahshan, K.A. Aly, Mater. Res. Express **6**(2), 025204 (2019)

15. S.S. Fouad, G.A.M. Amin, M.S. El-Bana, J. Non Cryst. Solids **481**, 314–320 (2018)

16. E.R. Shaaban, Y.A.M. Ismail, H.S. Hassan, J. Non Cryst. Solids **376**, 61–67 (2013)

17. M.F. Thorpe, J. Phys. C Solid State Phys. **6**(4), L75–L77 (1973)

18. E.A. Davis, N.F. Mott, Philos. Mag. J. Theor. Exp. Appl. Phys. **22**(179), 0903–0922 (1970)

19. L. Tichy, H. Ticha, P. Nagels, R. Callaerts, J. Non Cryst. Solids **240**(1–3), 177–181 (1998)

20. K.A. Aly, A. Dahshan, A.M. Abousehly, Phil. Mag. **88**(1), 47–60 (2008)

21. A.S. Hassanien, I. Sharma, Optik **200**, 163415 (2020)

22. N.F. Mott, E.A. Davis, R.A. Street, Philos. Mag. **32**(5), 961–996 (1975)

23. A.M. Adam, E. Lilov, E.M.M. Ibrahim, P. Petkov, L.V. Panina, M.A. Darwish, J. Mater. Process. Technol. **264**, 76–83 (2019)

24. K.A. Aly, A.M. Abousehly, M.A. Osman, A.A. Othman, Phys. B **403**(10–11), 1848–1853 (2008)

25. A.S. Soltan, M. Abu El-Oyoun, A.A. Abu-Sehly, A.Y. Abdel-Latief, Mater. Chem. Phys. **82**(1), 101–106 (2003)

26. S.H. Wemple, M. DiDomenico, Phys. Rev. B **3**(4), 1338–1351 (1971)

27. S.H. Wemple, Phys. Rev. B **7**(8), 3767–3777 (1973)

28. K. Tanaka, Thin Solid Films **66**(3), 271–279 (1980)

29. A.K. Walton, T.S. Moss, Proc. Phys. Soc. **81**(3), 509–513 (1963)

30. A.S. Hassanien, A.A. Akl, Phys. B Condens. Matter **576**, 411718 (2020)

31. P. Halevi, F. Ramos-Mendieta, Phys. Rev. Lett. **85**(9), 1875–1878 (2000)

32. C.C. Wang, Phys. Rev. B **2**(6), 2045–2048 (1970)

33. J.J. Wynne, Phys. Rev. **178**(3), 1295–1303 (1969)

34. H. Tichá, L. Tichý, J. Optoelectron. Adv. Mater. **4**(2), 381–386 (2002)

35. T.S. Moss, Phys. Status Solidi B Basic Res. **131**(2), 415–427 (1985)

36. N.M. Ravindra, V.K. Srivastava, Infrared Phys. **19**(5), 603–604 (1979)

37. A. Lamichhane, N.M. Ravindra, Energy gap–refractive index relations in Perovskites. Materials (Basel, Switzerland) **13**(8), 1917 (2020)